Since January 2020 Elsevier has created a COVID-19 resource centre with free information in English and Mandarin on the novel coronavirus COVID-19. The COVID-19 resource centre is hosted on Elsevier Connect, the company's public news and information website.

Virology 468-470 (2014) 490–503

Contents lists available at ScienceDirect

Virology

journal homepage: www.elsevier.com/locate/yviro

Inhibition of host extracellular signal-regulated kinase (ERK) activation decreases new world alphavirus multiplication in infected cells

Kelsey Voss [a], Moushimi Amaya [a], Claudius Mueller [b], Brian Roberts [c], Kylene Kehn-Hall [a], Charles Bailey [a], Emanuel Petricoin III [b], Aarthi Narayanan [a,*]

[a] National Center for Biodefense and Infectious Diseases, School of Systems Biology, George Mason University, 10650 Pyramid Place, Manassas, VA, USA
[b] Center for Applied Proteomics and Personalized Medicine, George Mason University, 10900 University Boulevard, Manassas, VA, USA
[c] Leidos Health Life Sciences, 5202 Presidents Court, Suite 110, Frederick, MD, USA

ARTICLE INFO

Article history:
Received 20 May 2014
Returned to author for revisions
31 August 2014
Accepted 6 September 2014
Available online 27 September 2014

Keywords:
ERK
Extracellular signal-regulated kinase
Alphavirus
Kinase
MAPK
Ag-126

ABSTRACT

New World alphaviruses belonging to the family Togaviridae are classified as emerging infectious agents and Category B select agents. Our study is focused on the role of the host extracellular signal-regulated kinase (ERK) in the infectious process of New World alphaviruses. Infection of human cells by Venezuelan equine encephalitis virus (VEEV) results in the activation of the ERK-signaling cascade. Inhibition of ERK1/2 by the small molecule inhibitor Ag-126 results in inhibition of viral multiplication. Ag-126-mediated inhibition of VEEV was due to potential effects on early and late stages of the infectious process. While expression of viral proteins was down-regulated in Ag-126 treated cells, we did not observe any influence of Ag-126 on the nuclear distribution of capsid. Finally, Ag-126 exerted a broad-spectrum inhibitory effect on New World alphavirus multiplication, thus indicating that the host kinase, ERK, is a broad-spectrum candidate for development of novel therapeutics against New World alphaviruses.

Introduction

The New World alphaviruses, Venezuelan equine encephalitis virus (VEEV), Eastern equine encephalitis virus (EEEV), and Western equine encephalitis virus (WEEV), can infect humans and potentially cause encephalitic disease (Weaver and Reisen, 2010). In 2013, Latin America recorded multiple confirmed cases of New World alphavirus infections with a total of 19 patients hospitalized for encephalitis. Among them, 3 patients died, 1 of whom had confirmed VEE (Carrera et al., 2013). Owing to their propensity to cause naturally-occurring disease, these alphaviruses have been classified as emerging infectious agents. The New World alphaviruses have the potential to be extremely infectious by the aerosol route and have therefore been explored previously as potential bioweapons (Zacks and Paessler, 2010). For this reason, VEEV and EEEV are classified by the Centers for Disease Control (CDC) as Category B select agents. There are currently no FDA-approved therapeutic candidates or vaccines for the protection of humans from New World alphavirus infections. The attenuated TC-83 strain of VEEV is used to vaccinate select at-risk personnel; however, TC-83 has concerns regarding safety and is considered to be a reactogenic vaccine (Barrett and Stanberry, 2009). Around 40% of all vaccinees have developed disease with some symptoms typical to that of natural VEE infection (Volkova et al., 2008). Therefore, there are ongoing efforts to establish a more effective and safer vaccine, some of which include vaccine candidates derived from the V3526 attenuated strain of VEEV (Fine et al., 2010; Martin et al., 2010; Paessler and Weaver, 2009; Sharma et al., 2011). FDA-approved antiviral therapies for RNA viruses, such as ribavirin, have been ineffective against VEEV and WEEV (Canonico et al., 1984), further highlighting the importance of new therapeutic approaches as medical countermeasures against New World alphaviruses.

Viruses rely on their host cell for the establishment of a productive infectious cycle. Viruses are obligate pathogens that are known to modulate and utilize many host events, including host signal-transduction mechanisms. A deeper understanding of the dynamics of the interactions between the host and the pathogen can help in the identification of novel targets for therapeutics. For example, many alphaviruses have developed the ability to interfere with the induction of the host cell antiviral response (Burke et al., 2009; Garmashova et al., 2007). Animal models have also revealed changes in gene expression in VEEV-infected mouse brains (Sharma et al., 2008). We have demonstrated that host kinases, such as

* Correspondence to: National Center for Biodefense and Infectious Diseases, George Mason University, Biomedical Research Lab, 10650 Pyramid Place, MS 1J5, Manassas, VA 20110, USA. Tel.: +703 993 9610; fax: +703 993 4280.
E-mail address: anaraya1@gmu.edu (A. Narayanan).

http://dx.doi.org/10.1016/j.virol.2014.09.005
0042-6822/

glycogen synthase kinase-3β (GSK-3β) and the inhibitor of nuclear factor kappa-B kinase subunit beta (IKK-β), were modified upon VEEV infection (Kehn-Hall et al., 2012; Amaya et al., 2014). Targeting these kinases with small molecule inhibitors resulted in a decrease of viral replication. Such observations underscore the potential of host-based candidates as therapeutic targets for development of antivirals against New World alphaviruses. The advantages conferred by host-based therapeutics include a decreased potential for the development of resistant strains and an increased probability of broad-spectrum applicability to treat many viral indications. The concerns around host-based therapeutics include a low threshold for toxicity and hence, a requirement of a stringent analysis of inhibitor induced toxicity profiles in the host.

The host MAPK, extracellular signal-regulated kinase (ERK), responds to stress events including infection by directing multiple downstream events like inflammation and cell death (Hong et al., 2009; Hu et al., 2004; Xing et al., 2010). ERK exists as ERK1 and ERK2 (hereafter referred to collectively as ERK1/2), both of which have a central position in the MAPK cascade, downstream in RAS-RAF-MEK-ERK signal transduction (Roskoski, 2012a, 2012b). Briefly, RAF kinases act by phosphorylating and therefore activating MEK1 and MEK2 (collectively referred to as MEK1/2). MEK1/2 have dual specificity for ERK1/2, phosphorylating first at tyrosine and then threonine sites in the activation segments of ERK1/2, causing subsequent activation (Roskoski, 2012a, 2012b). Activated ERK1/2 act as protein-serine/threonine kinases, phosphorylating more than 150 cytosolic and nuclear substrates (Yoon and Seger, 2006; Shaul and Seger, 2007). ERK1/2 form an activated dimer and translocate to the nucleus, where they phosphorylate transcription factors regulating gene transcription (Chuderland and Seger, 2005; Parra et al., 2005).

Multiple viruses are known to activate the RAS–RAF–MEK–ERK signaling cascade in the host cell, and in many cases, this activation has been correlated with viral replication (Pleschka, 2008). Specifically, publications have implicated the ERK signaling pathway in the regulation of viral replication and gene expression for Coxsackievirus B3 (Luo et al., 2002), human cytomegalovirus (Boldogh et al., 1990; Johnson et al., 2001), Junin virus (Rodríguez et al., 2014), human immunodeficiency type 1 (Furler and Uittenbogaart, 2010; Jacqué et al., 1998), coronavirus (Cai et al., 2007), and influenza virus (Pleschka et al., 2001). Of particular relevance to our studies, it was reported that Borna disease virus, an RNA virus with high neurotropism, also manipulates the RAF/MEK/ERK signaling cascade in vitro and appears to be essential for viral spread (Hans et al., 2001; Planz et al., 2001). Here we demonstrate that VEEV infection of human astrocytoma cells results in the phosphorylation of multiple target proteins in the ERK signaling cascade. Using a small molecule inhibitor of ERK, Ag-126, we demonstrate that ERK1/2 phosphorylation plays an important role in VEEV multiplication in infected cells. We provide data which suggest that early and late events in the viral infectious cycle are susceptible to ERK1/2 inhibitors. We extend our studies to the virulent strains of VEEV, WEEV and EEEV, and demonstrate that ERK1/2 signaling is a broad-spectrum requirement for New World alphaviruses for the establishment of a productive infectious cycle.

Results

The RAF/MEK/ERK signaling cascade Is activated in VEEV-infected cells

Our previous studies have indicated that host kinases including IKK-β and GSK-3β were modulated in VEEV-infected cells and that inhibition of these kinases with small molecule inhibitors resulted in decreased viral multiplication (Amaya et al., 2014; Kehn-Hall et al., 2012). We reported in our IKK-β study that multiple components,

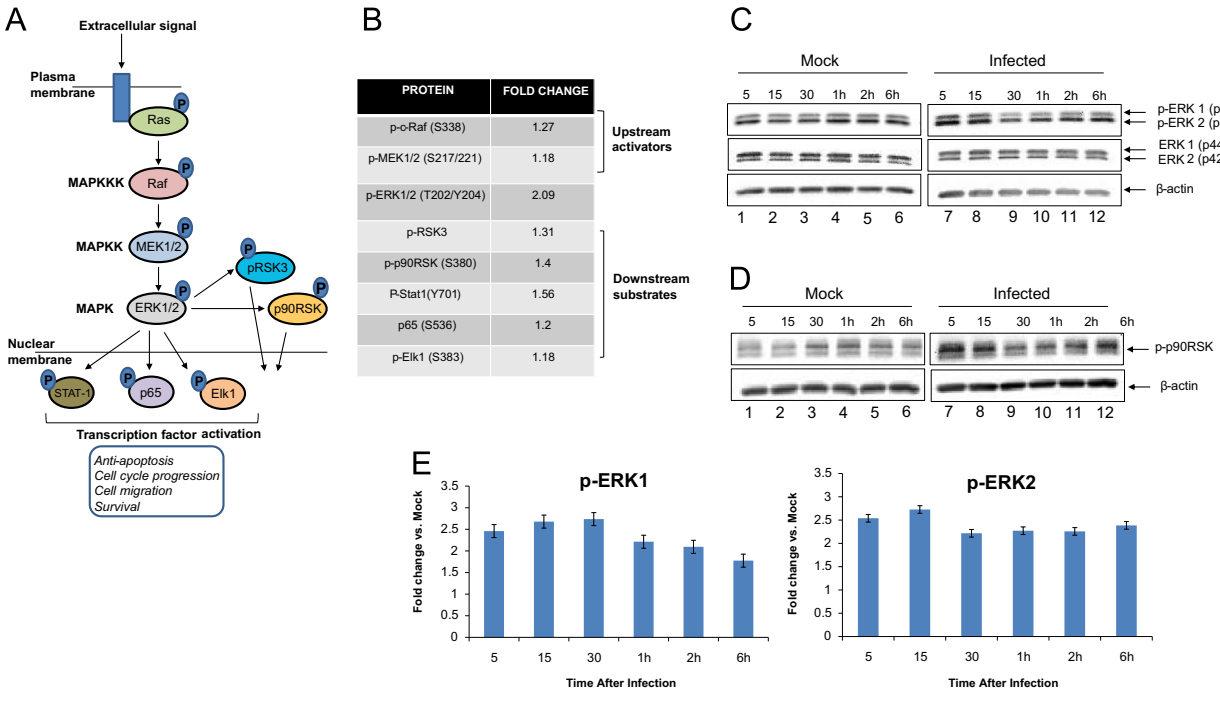

Fig. 1. ERK1/2 signaling is activated in TC-83 infected cells (A) Schematic of ERK signal transduction cascade – upstream activators and downstream targets. (B) Quantification of fold changes in phosphorylation status of target proteins in infected cells over uninfected cells as observed by RPPA. Signal intensities pertaining to phosphorylated forms of proteins were calculated for mock-infected lysates and TC-83 infected lysates following imaging and quantification of the RPPA slides. The values were then used to calculate the fold change in phosphorylation in the infected samples over the mock-infected samples. (C) Western blot validation of ERK phosphorylation in U87MG cells after infection with TC-83. Infected and mock uninfected cell lysates were collected at the time points indicated. β-actin was used as a loading control, and three independent experiments were conducted. (D) Western blot validation of downstream substrate p90RSK phosphorylation. (E) Quantification p-ERK1 and p-ERK2 in infected cells from three independent experiments, normalized to β-actin and then compared to the mock at each time point. Bars indicate the mean and error bars represent standard error.

which collectively constitute the NFkB response (IKK-β, IκBα, p65), were phosphorylated as part of a cascade activation process (Amaya et al., 2014). Based on our previous lines of evidence, we hypothesized that VEEV infection will activate other host phospho-signaling cascades in infected cells and inhibition of specific events in those cascades will have an effect on VEEV multiplication. We utilized a reverse phase protein microarray (RPPA) approach to identify changes in phospho-signaling cascades in VEEV-infected cells. We have successfully used this approach in previous studies to identify host events that are altered in virus-infected cells (Popova et al., 2010a, 2010b; Wulfkuhle et al., 2006). The RPPA analysis was carried out as described previously (Popova et al., 2010a, 2010b). Briefly, U87MG cells were either mock infected or infected with TC-83, the attenuated strain of VEEV. Infections with TC-83 as indicated throughout the manuscript involved exposure of the cells to the virus for one hour unless otherwise indicated. We are referring to as the time frame during which infection was allowed to happen after which the viral overlay was removed. The antibodies used for the analysis included a diverse range of signaling cascades such as growth factor signaling, Akt signaling, NFkB signaling, and ERK signaling. Fold differences in phosphorylation of the candidate proteins seen in infected cells were calculated in comparison with those in the uninfected cells. We observed that multiple signaling molecules, which are part of the RAS–RAF–MEK–ERK signaling cascade, were phosphorylated in VEEV-infected cells. The schematic of the ERK signaling cascade is shown in Fig. 1A. The RPPA analysis revealed that levels of phosphorylated ERK1/2 were 2-fold higher in infected cells when compared with uninfected cells (Fig. 1B). The data also indicated that the phosphorylation of the ERK1/2 upstream activator MEK1/2 was also increased (Fig. 1B). Furthermore, many downstream targets of ERK1/2 including Elk-1 (Cruzalegui et al., 1999), p65 (Carter and Hunninghake, 2000), and Stat-1 (Zhang et al., 2004) were activated in infected cells (Fig. 1B). Cumulatively, preliminary RPPA data indicated that the ERK signaling cascade was activated in VEEV-infected cells.

We performed independent validation experiments with a focus on the phosphorylation status of ERK1/2 in TC-83 infected U87MG cells. We carried out infections of U87MG cells and collected total protein lysates at multiple time points between 5 min after the removal of initial viral inoculum (referred to hence forth as the infection period) and 6 h after the infection period. The lysates were subsequently fractionated by SDS-PAGE and analyzed by Western blot using antibodies against phosphorylated ERK1/2 (Thr202/Tyr204), unphosphorylated (total) ERK1/2, and β-actin. The results showed an increased phosphorylation of ERK1/2 in the infected cells after the infection period (Fig. 1C, compare lanes 1 and 7). Levels of p-ERK1/2 remained consistently higher in the infected samples than the mock samples for the entire time course which distinguished the phospho-profile of ERK1/2 in infected cells from the mock-infected control cells (Fig. 1C). We performed additional validation experiments of the RPPA data by subjecting our protein lysates to Western blot using antibodies against p-p90RSK and β-actin. The activation profile of p90RSK paralleled that of ERK1/2 and agreed with the data obtained by the RPPA process (Fig. 1D). To quantify levels of p-ERK1/2 in the TC-83 infected samples, three independent experiments were performed and the fold changes over the mock samples in each experiment averaged. Levels of p-ERK1 and p-ERK2 remained at around a minimum of a 2-fold increase over the mock throughout the time course (Fig. 1E). Our analysis of total ERK1/2 levels did not indicate any significant differences between mock and infected samples, thus indicating the phosphorylation event to be independent of total protein levels. Cumulatively, the data included in Fig. 1 suggest that infection of U87MGs with the attenuated TC-83 strain of VEEV results in an activation of the ERK signaling cascade and phosphorylation of ERK1/2 at early time points after infection.

Inhibition of ERK1/2 phosphorylation with Ag-126 inhibits viral multiplication

Following validation of ERK phosphorylation in VEEV-infected cells, we wanted to determine if this phosphorylation event was essential for viral replication. To define the role of ERK1/2 in TC-83 infection, an inhibitor of ERK1/2 phosphorylation, tyrphostin Ag-126, was employed. Tyrphostin Ag-126 (α-cyano-[3-hydroxy-4nitro]cinnamonitrile), has been reported as a cell-permeable inhibitor of lipopolysaccharide (LPS)-induced synthesis of tumor necrosis factor–alpha (TNF-α) and nitric oxide (NOS) in murine peritoneal macrophages (Novogrodsky et al., 1994). It also blocks LPS-induced tyrosine phosphorylation of ERK and its substrates and reduces the expression of iNOS and COX-2 in the lungs of rats treated with carrageenan (Chatterjee et al., 2003). Before we evaluated the antiviral efficacy of Ag-126, we determined the toxicity profile of Ag-126. U87MG cells were seeded in 96-well plates and 24 h later, increasing concentrations of Ag-126 were added to wells in triplicate. DMSO was added as a negative solvent control. The cells were maintained in the presence of Ag-126 for 24 h after which viable cells were quantified by measuring luminescence in a Cell-Titer-Glo assay. The assay results showed that the inhibitor was non-toxic to U87MG cells when compared to the DMSO treated cells at the concentration range tested (Fig. 2A). For all our subsequent experiments, we have used Ag-126 at a concentration of 10 μM unless otherwise indicated.

As a next step, we wanted to test whether inhibiting ERK1/2 phosphorylation with Ag-126 would have an effect on TC-83 replication. U87MG cells were plated in a 96-well format and were pretreated for 2 h with Ag-126. The media with the inhibitor was removed and cells were infected with TC-83 for 1 h at 37 °C. The viral overlay was removed at the 1 h time frame and media with Ag-126 was added back to the cells. The cells were then incubated for up to 24 h at 37 °C after which the supernatants were collected to quantify infectious viral titers using plaque assays. Controls included infected cells treated with DMSO. As the concentration of Ag-126 treatment increased, the amount of viral inhibition increased, demonstrating a dose-dependent response (Fig. 2B). To determine whether the inhibitory effects of Ag-126 were dependent on the multiplicity of infection (MOI), U87MG cells were pretreated for 2 h with Ag-126 or DMSO alone and infected with TC-83 at three different MOIs (0.1, 0.5, 1). The cells were incubated for 24 h as described previously and the supernatants were collected for quantification of infectious viral titers. Our data indicated that even at higher viral titers, Ag-126 continued to be inhibitory to viral multiplication (Fig. 2C).

To assess the effect of Ag-126 on expression of viral proteins, whole cell lysates were obtained at 8 and 24 h post-infection, and subjected to Western blot analysis using antibodies to VEEV capsid and envelope glycoproteins. At 8 h post-infection (8 hpi), VEEV capsid protein can be detected in the treated cells; however, the amount of capsid protein detected at this time point in the untreated cells was higher in the untreated cells (Fig. 2D, compare lanes 1 and 2). The difference between the amounts of capsid protein produced in Ag-126 treated versus untreated cells was more prominent at the 24 h time point (compare lanes 3 and 4). While we were unable to detect the VEEV E2 glycoprotein (GP) at 8 hpi, we could detect fairly robust expression of glycoprotein in TC-83 infected, untreated cells when compared to treated cells at the 24-hour time point (Fig. 2D, lanes 3 and 4). We quantified the differences of treated and untreated cells at the 24-hour time point in two independent experiments and found that Ag-126 treatment modestly reduced capsid expression, and had a greater effect on GP expression (Fig. 2D). This indicated that decrease in viral structural protein levels by Ag-126 treatment may be partially responsible for decreased viral titers. We also conducted Western blot analysis on infected and Ag-126 treated and infected cell lysates to

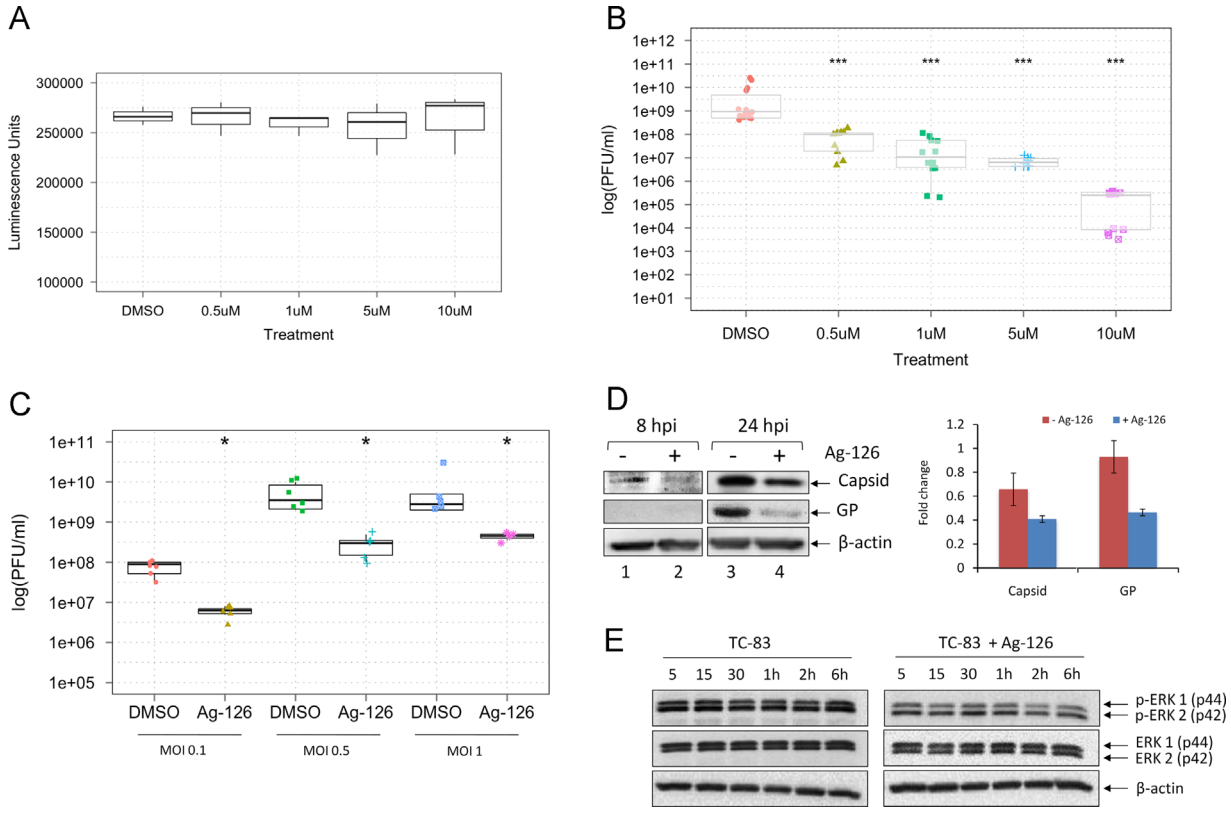

Fig. 2. Inhibition of ERK1/2 phosphorylation reduces TC-83 replication and leads to lowered virus protein expression. (A) U87MG cells were treated with Ag-126 for 24 h, and the Cell-Titer-Glo assay was conducted. Luminescence was measured and the values indicated as luminescence units in the *Y*-axis. The concentrations of the drug that were used in this experiment are indicated in the *X*-axis. DMSO alone was used as a negative control, at 0.1% concentration. (B) U87MGs were pretreated Ag-126 for 2 h. Cells were infected with TC-83 for one hour (MOI:0.1). The conditioned media was then added back onto the cells and 24 hpi the supernatants were collected. The graph portrays the results of three independent experiments. (C) Cells were treated with 10 μM Ag-126 or DMSO alone and infected at either an MOI of 0.1, 0.5, or 1. Conditioned media was added back to the cells after the one hour infection period, and left until supernatants were collected at 24 hpi. (D) Whole cell lysates were obtained from U87MG cells after infection with TC-83 (MOI:1). Cells were infected in the presence or absence of Ag-126 treatment (10 μM). Infected cell lysates were collected at 8 hpi and 24 hpi. Amounts of β-actin were used as a loading control. Data in the bar graph is representative of duplicate experiments at the 24 hpi time point. (E) Cells were infected with TC-83 (MOI:1) and either untreated or treated with Ag-126. Total protein lysates were obtained at the indicated time points and analyzed by Western blot for phosphorylation status of ERK1/2.

ensure that Ag-126 treatment did indeed inhibit phosphorylation of ERK1/2. Using antibodies against phosphorylated ERK1/2 (Thr202/Tyr204), unphosphorylated (total) ERK1/2, and β-actin, we were able to document a decrease in the amount of phosphorylated ERKs at all time points tested in the presence of Ag-126 (Fig. 2E).

We performed a similar inhibition efficacy study in Vero cells to determine if the inhibition we observed in U87MG cells was a cell type dependent phenomenon. To that end, we first evaluated the cytotoxicity of Ag-126 in Vero cells and determined that up to 50 μM concentrations, Ag-126 did not evoke any cytotoxic responses (Fig. 3A). We then determined if Ag-126 could inhibit TC-83 multiplication in Vero cells by pretreating cells with Ag-126 for 2 h and then infecting with TC-83. Infectious titers were measured by plaque assays at 24 h post the infection period. The result shown in Fig. 3B indicates that Ag-126 could inhibit TC-83 even in a permissive cell line such as Vero cells, albeit, the extent of inhibition being lesser than what we observed in U87MG cells. Cumulatively, our data suggested that at nontoxic concentrations, Ag-126 inhibited ERK1/2 phosphorylation, decreased viral protein expression and negatively influenced TC-83 multiplication in infected cells.

Inhibition of ERK1/2 phosphorylation with Ag-126 inhibits nuclear accumulation of ERK, but does not interfere with nuclear accumulation of VEEV capsid protein

Phosphorylated ERK1/2 has both nuclear and cytosolic targets, but typically is known to dimerize and translocate to the nucleus where it acts on multiple transcription factors (Roskoski, 2012a). Inhibition of ERK1/2 phosphorylation by small molecule inhibitors affected nuclear translocation of ERK1/2 (Roskoski, 2012a). Therefore, to confirm that Ag-126 treatment indeed resulted in decreased phosphorylation of ERK1/2 in U87MG cells, we investigated the intracellular p-ERK1/2 localization during VEEV infection in the presence or absence of Ag-126 at different time points using confocal microscopy as described previously (Amaya et al., 2014). Briefly, U87MG cells were seeded in 8-well chambered slides and infected with TC-83 virus. At 6 and 24 h after the infection period, the cells were fixed and probed with antibodies to ERK1/2 and VEEV capsid. At 6 h, nuclear enrichment of p-ERK1/2 was observed in 71% of cells that were infected with TC-83 (Fig. 4A). We defined nuclear enrichment by a visual assessment, in which p-ERK1/2 was localized to the nucleus. In contrast, 38% of mock cells showed enrichment, whereas the Ag-126 treated cells had 22% enrichment. Therefore, treatment with Ag-126 resulted in a decrease in nuclear p-ERK1/2, thus attesting to an inhibition of ERK phosphorylation. This observation added support to the data presented in Fig. 2E.

At 24 h, 30% of TC-83 infected cells demonstrated a nuclear enrichment of p-ERK1/2, but only 16% of the mock-infected cells showed nuclear ERK1/2 (Fig. 4B). Capsid staining was detected in 90% of cells exposed to TC-83 virus, but not treated with Ag-126. In comparison, capsid staining was reduced by 68% in the infected, Ag-126 treated cells. While overall capsid staining was reduced in Ag-126 treated cells, we did not observe any difference in the

distribution of capsid between the nucleus and cytoplasm of infected cells, regardless of Ag-126 treatment thus indicating that ERK1/2-mediated signaling events did not play a role in the nuclear-cytoplasmic transport of VEEV capsid protein in infected cells. Cumulatively, our microscopy studies, while attesting to the inhibitory action of Ag-126 in negatively influencing the nuclear accumulation of ERK1/2, did not support the potential of ERK-mediated phosphorylation to control nuclear-cytoplasmic transport of VEEV capsid protein.

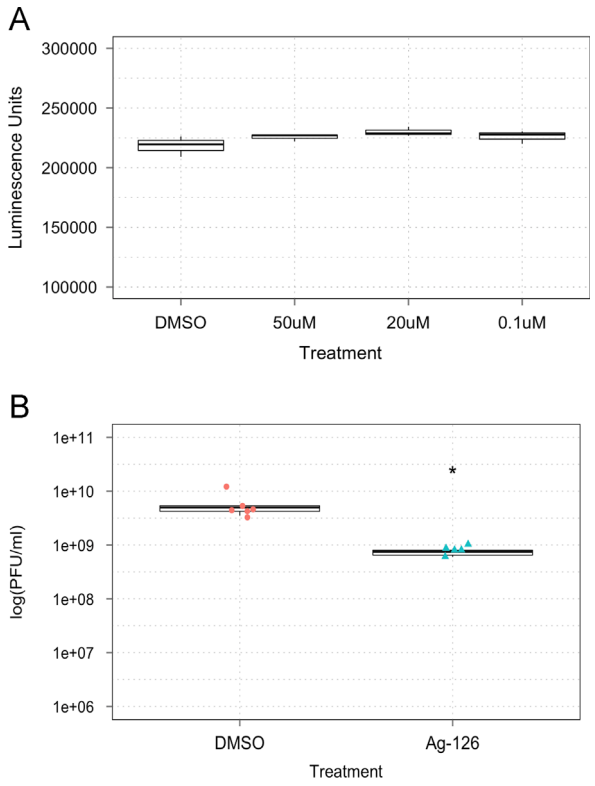

Fig. 3. Inhibition of ERK1/2 phosphorylation with Ag-126 is not cell type dependent. (A) VERO cells were seeded at 30,000 cells per well in a 96-well plate and different concentrations of Ag-126 applied. Cell-Titer-Glo assay was performed the next day. (B) VERO cells seeded at 10,000 cells per well in a 96-well plate were pre treated for 2 h with Ag-126 (50 μM) and infected with TC-83 (MOI:0.1) for one hour. Conditioned media was replaced and supernatants collected at 24 hpi were subjected to plaque assay.

Treatment with Ag-126 interferes with viral replication kinetics

Our study thus far, has analyzed inhibition of TC-83 multiplication by Ag-126 as a static phenomenon, at 24 h after the infection period. It would be more informative to determine if the overall replication kinetics of the virus was impacted by Ag-126 treatment. To this end, U87MG cells were pre-treated with Ag-126 for 2 h or DMSO alone as a control. Cells were infected with TC-83, supernatants were collected at multiple time points (3, 6, 16, 24 and 30 h post-infection), and plaque assays were performed. The results, as shown in Fig. 5A, demonstrate an overall decrease in viral replication kinetics that could be clearly observed as early as 6 h post the infection period and was not exacerbated over subsequent time points. We performed time-of-addition experiments in an attempt to identify specific time frames in the infectious cycle when the inhibition by Ag-126 could be detected. Cells were treated with either Ag-126 or DMSO alone, at the indicated times (Fig. 5B). All supernatants were collected at 24 h and quantified for infectious viral titers. We observed that when cells were pretreated with Ag-126 two hours before infection (2 h pre), robust inhibition was apparent. While Ag-126 continued to be inhibitory when added 2 hpi (2 h post), the extent of inhibition was not as robust as the 2-hour pretreatment. When the drug was added at 4 hpi, the inhibitory potential decreased (Fig. 5C). We also observed a modest, but statistically significant reduction in titers when drug was added at 8 h post the infection period, which could potentially implicate Ag-126 in late events as well. However, it is unclear whether the apparent inhibition seen at the 8 h time point was due to late events in the first round of viral multiplication, or the early events of the second round of multiplication. Cumulatively, our experimentation with the addition of Ag-126 at

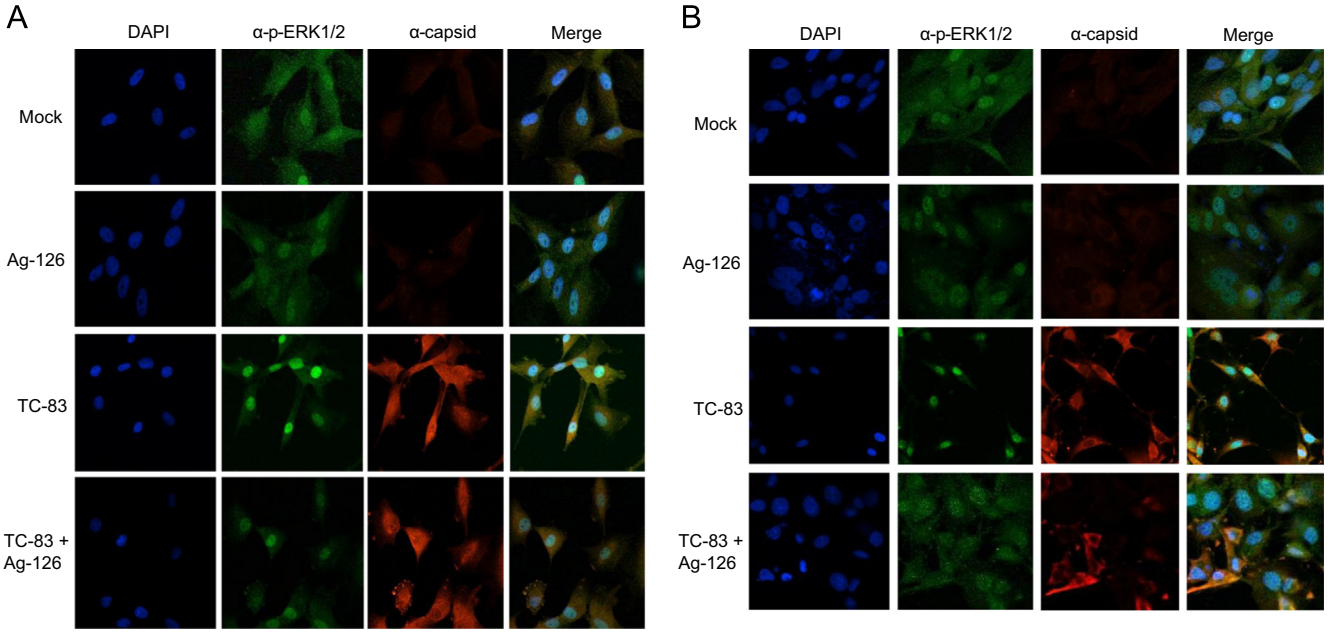

Fig. 4. Ag-126 treatment decreases nuclear pools of p-ERK1/2 without influencing capsid localization in the nucleus. U87MG cells were seeded in a 8-chambered slide and infected with TC-83 (MOI:1). For every variable, at least two independent wells were analyzed. Cells were fixed at 6 (A) and 24 (B) hpi and stained with antibodies against VEEV capsid (red) and p-ERK1/2 (green). The slides were also stained with DAPI to stain the nucleus (blue). Images were collected using a Nikon Eclipse TE2000-U and acquired with a 60X objective. Images are representative of multiple fields that were imaged for each variable. Three independent experiments were conducted.

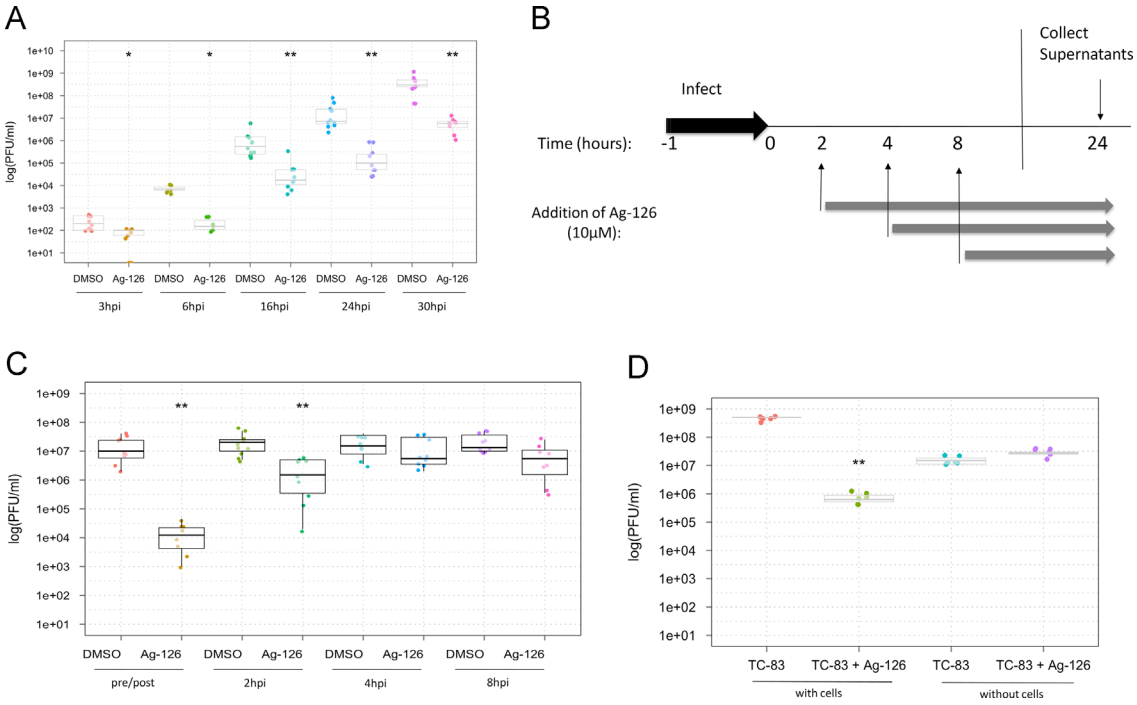

Fig. 5. Ag-126 treatment exerts an inhibitory effect on viral replication kinetics during the early stages of the infectious process. (A) U87MG cells were seeded in 96-well plates and treated with Ag-126 (10 μM). Cells treated with DMSO were maintained as controls. The cells were infected with TC-83 (MOI:0.1) and supernatants were obtained at multiple time points after infection and quantified by plaque assays. The *Y*-axis indicates the PFU/ml titer of infectious virus and the *X*-axis indicates the time points at which supernatants from drug/DMSO treated cells were analyzed. (B) Time of addition study - Ag-126 was added to U87MG cells either at 2 h prior to infection or at 2, 4, and 8 hpi. All infections took place at the same time, for one hour (MOI:0.1). The gray arrows indicate presence of Ag-126 in different samples (2, 4, and 8 hpi). Supernatants from all conditions were collected at 24 hpi and quantified by plaque assays. (C) *Y*-axis refers to titers of infectious virus and *X*-axis indicates the time points at which drug was introduced. Pre/post indicates a 2 h pretreatment, and replacement of media with inhibitor after the one hour infection period. The experiment was conducted 4 independent times. (D) TC-83 was incubated directly with Ag-126 for 1 h in the absence of cells prior to quantification by plaque assays (without cells). As a control, U87MG cells were infected with TC-83 in the presence of Ag-126 (with cells). Plaque assays were performed with VERO cells using supernatants from both conditions for quantification of infectious virions. Differences between TC-83 and TC-83+Ag-126 without cells was not statistically significant. (E) Detailed time of addition assay schematic. (F) Time of addition outcomes are indicated. *Y*-axis indicates infectious viral titers and *X*-axis indicates time frames when Ag-126 was present. Results from three independent experiments are shown in the figure.

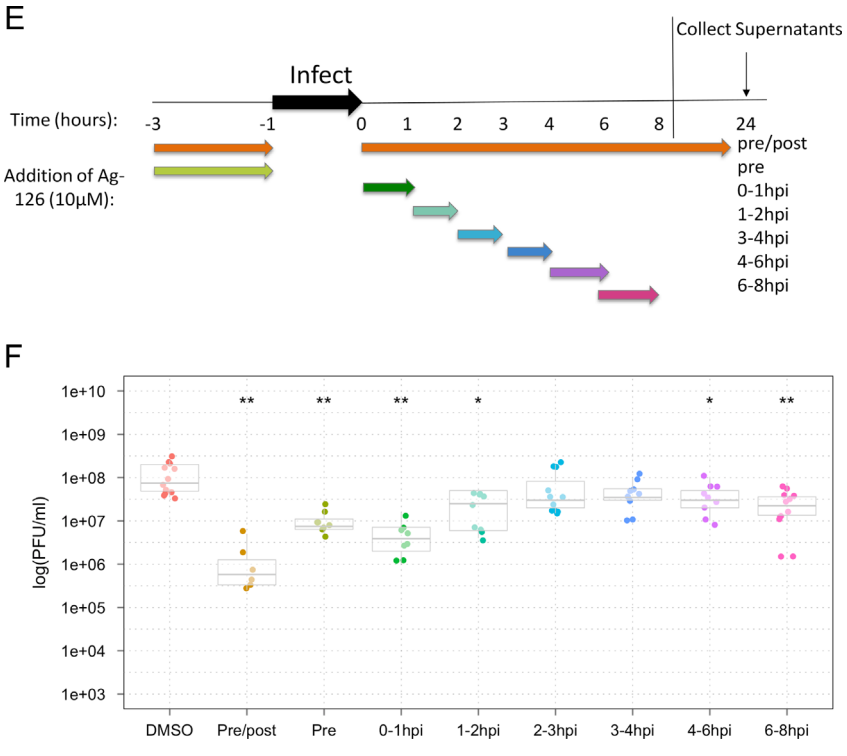

Fig. 5. (*continued*)

multiple time points after the infection period revealed that Ag-126 may affect viral multiplication at early and late time frames of the infectious process. The fact that the pretreatment strategy was the most efficacious in our hands could also imply that the longer the drug is available in the system, the greater the extent of inhibition observed.

At this time, we wanted to determine if Ag-126 was directly virucidal in nature, which may also contribute to the observed inhibition with a concentration towards the early time points. To address this possibility, we performed a modified plaque reduction neutralization assay. We incubated TC-83 directly with Ag-126 for 1 h at room temperature. After the incubation, the infectivity of the virus was quantified by plaque assay. Our data indicated that when Ag-126 was added to U87MG cells in the presence of virus, there was inhibitory action as expected; this acted as our positive control for the inhibitory potential of Ag-126 (Fig. 5D). However, when we incubated the virus directly with Ag-126 as a part of the same experiment, in the absence of U87MG cells and then quantified the infectivity of the virus by plaque assay, there was no difference between virus exposed to the drug and virus not exposed to the drug, thus indicating that Ag-126 did not exert any direct virucidal activity.

To gain more insight into the antiviral effects of Ag-126 on TC-83 multiplication, we performed a slight variation of the time of addition study in which the drug was made available only for limited blocks of time. This experimental organization involved adding the drug at different time points followed by removing the drug and replacing with fresh media (Fig. 5E). U87MG cells were treated with Ag-126 at the indicated times and all supernatants were collected at 24 h and quantified for infectious viral titers (Fig. 5E). We observed that when cells were pre treated for 2 h (pre), there was a robust inhibition of TC-83 (Fig. 5F). However, the inhibition was even more robust when the drug was added directly after the one hour infection period for one hour (0–1 hpi). Later time points were modestly efficacious. Paralleling our earlier observation, addition of the drug at the 6–8 h window resulted in a statistically significant decrease in viral multiplication. This may be due to the influence of Ag-126 on late stages of viral multiplication or reflective of the early events during the second round of viral multiplication.

Treatment with Ag-126 decreases the amount of VEEV glycoprotein in the endoplasmic reticulum

We attempted to determine whether inhibition of viral multiplication by Ag-126 may also be a result of aberrant transport and/or localization of structural proteins such as the glycoproteins to the endoplasmic reticulum (ER) and the golgi apparatus (Snyder and Mukhopadhyay, 2012). To that end, we performed confocal microscopy experiments using antibodies to the ER and the golgi apparatus in the context of TC-83 infection, with and without Ag-126 to assess glycoprotein distribution in the ER and Golgi. We carried out this experiment using VEEV glycoprotein antiserum and analyzed the distribution of the glycoprotein in the ER and golgi at 1, 2, 4 and 6 h post the infection period. In our hands, we were able to detect glycoprotein in the ER at the 1 h time point and the ER signal steadily decreased during the time course of analysis (Fig. 6A and B). We were not able to observe any distinct colocalization of glycoprotein with the golgi apparatus within the time frames included in our study (Fig. 6A). In the presence of Ag-126, we noticed that the glycoprotein signal in the ER was reduced at the 1 h time point and the difference in the ER signal between the treated and untreated cells increased by the 2 and 4 h time points suggesting that Ag-126 may have an effect on the ER localization of VEEV glycoprotein.

Activation of ERK1/2 increases viral replication of VEEV

We hypothesized that if inhibition of ERK1/2 activation resulted in down-regulation of VEEV multiplication, activation/priming of ERK1/2 could contribute to an up-regulation of VEEV multiplication. We employed a MAPK activator of ERK, Ceramide

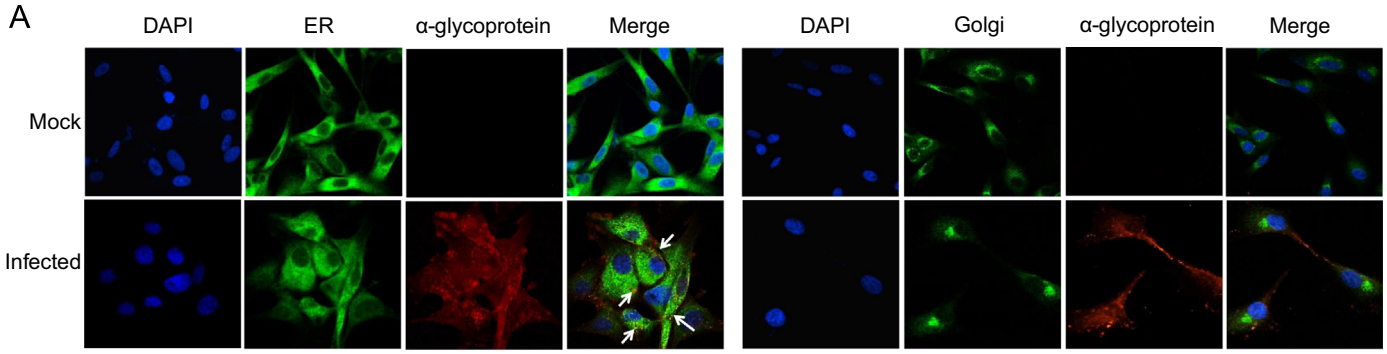

B

		1hpi:	2hpi:	4hpi:	6hpi:
TC-83	cells counted:	69	103	86	83
	infected:	36	39	52	59
	co-localization:	13	11	13	9
	% localization:	36.1	28.2	25	15.3
Ag-126 + TC-83	cells counted:	96	122	131	87
	infected:	51	53	82	53
	co-localization:	12	10	11	9
	%localization:	23.5	18.9	13.4	17.0

Fig. 6. Inhibition of ERK1/2 phosphorylation with Ag-126 results in less VEEV glycoprotein in the endoplasmic reticulum. U87MG cells were seeded in a 8-chambered slide and infected with TC-83 (MOI:1). For every variable, at least three independent wells were analyzed. (A) Cells were fixed at 1, 2, 4, and 6 hpi and stained with antibodies against VEEV glycoprotein (red) and an endoplasmic reticulum (ER) marker (green). The slides were also stained with DAPI to stain the nucleus (blue). Slides were also fixed and stained with a golgi marker (green) at the same time points. Images were collected using a Nikon Eclipse TE2000-U and acquired at 60× objective. Images are representative of multiple fields that were imaged for each variable. Two independent experiments were conducted. (B) Cells from triplicate wells in two experiments were counted at random for co-localization of VEEV glycoprotein and the ER in the presence and absence of Ag-126.

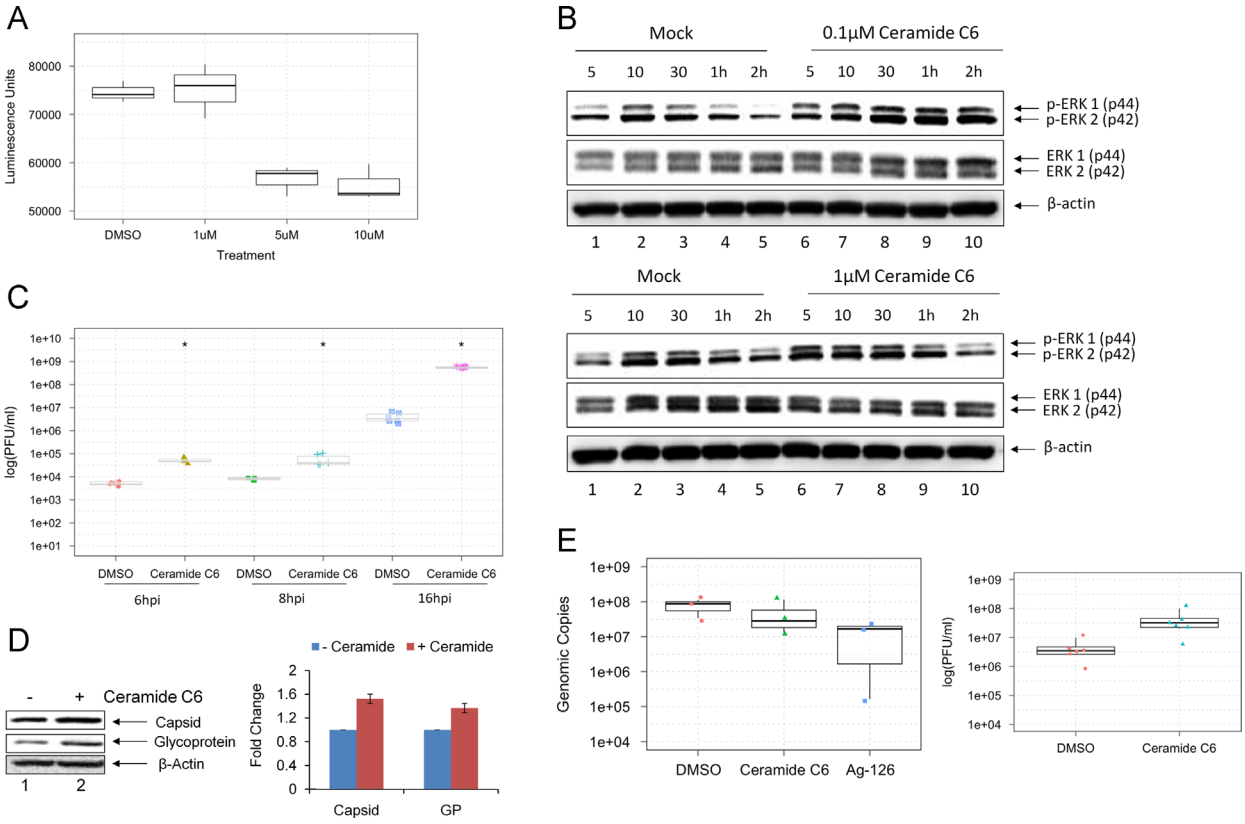

Fig. 7. Activation of ERK1/2 increases TC-83 replication kinetics. (A) U87MG cells were seeded in a 96-well plate, treated with Ceramide C6 for 24 h, and the Cell-Titer-Glo assay was conducted to quantify cell viability. Luminescence (indicated in the *X*-axis) was measured and indicates cell viability. *Y*-axis indicates the concentration of drug used. Mock and DMSO alone were used as controls. (B) Western blot analysis of 0.1 μM Ceramide C6 and 1 μM Ceramide C6 treatments on the phosphorylation status of ERK1/2. Lysates were collected at 5, 10, and 30 min post-treatment, and 1, 2 h post-treatment. (C) U87MG cells were pretreated with 0.1 μM Ceramide C6 for 2 h and then infected with TC-83 (MOI:0.1). Supernatants were collected at 6 hpi, 8 hpi, and 16 hpi (*X*-axis) and quantification of infectious virus (*Y*-axis) was performed by plaque assays. (D) Western blot analysis of Ceramide C6 treatment on viral proteins at 24 h post infection. Two independent experiments are averaged and shown as bars. (E) qRT-PCR results of VEEV genomic copies at 16 hpi. To the right, the supernatants from the same exact wells examined in the qRT-PCR for intracellular genomic copies were subjected to plaque assay to quantify infectious virus.

C6 (Raines et al., 1993), to prime the cells and activate ERK1/2 phosphorylation prior to infection. As a first step, we assessed the toxicity of the compound in U87MG cells and found no loss of viability at 1 μM concentration of the compound (Fig. 7A). Treatments greater than or equal to 5 μM, however, had a noticeable level of toxicity. Therefore, we decided to proceed with 0.1 μM treatments for analysis of viral replication kinetics when ERK was activated prior to infection. To validate that Ceramide C6 treatment was activating ERK1/2 under our experimental conditions, we collected whole cell protein lysates at multiple time points in the presence or absence of Ceramide C6 and performed Western blot analysis. The data indicated that Ceramide C6 treatment increased the amount of phosphorylated ERK1/2 at 0.1 μM and 1 μM treatments. Addition of 1 μM Ceramide C6 resulted in a earlier activation of ERK signaling (Fig. 7B, compare lanes 1 and 6), than 0.1 μM treatment confirming that Ceramide C6 does indeed activate ERK1/2 signaling in this cell type.

To determine if Ceramide C6-based activation of ERK prior to infection contributed to an increase in viral multiplication, U87MG cells were treated for 2 h with either DMSO alone or 0.1 μM Ceramide C6 and then infected with TC-83 for 1 h. Supernatants were collected at 6, 8, and 16 hpi and quantified by plaque assay. Our data indicated that virus titers were statistically significantly higher with Ceramide C6 treatments at the 6 h analysis point (Fig. 7C). By 16 h, the Ceramide C6-treated samples had more than a 2-log increase over the DMSO samples. We then assessed the effect of Ceramide C6 treatment on the expression of viral proteins. We saw a modest increase of VEEV capsid and glycoprotein (GP) when cells were treated with 0.1 μM Ceramide C6 before infection with TC-83 (Fig. 7D). Two independent experiments were conducted and protein levels normalized to β-actin quantified from both experiments. The average is shown by the bars in Fig. 7D.

We next wanted to determine if activation of ERK1/2 had an effect on the amount of viral RNA produced in the treated cells. To assess the levels of intracellular viral RNA, we performed quantitative RT-PCR (qRT-PCR) with VEEV specific primers. At 16 hpi, where we saw the greatest difference of infectious viral titers, we isolated intracellular RNA and subjected it to qRT-PCR analysis. The genomic copies did not show any noticeable differences in the viral RNA accumulation in the cells dependent on Ceramide C6 treatment (Fig. 7E). The supernatants that corresponded to the 16 h time point that was analyzed by the PCR method was subjected to plaque assay to quantify infectious virus in those same supernatant samples. Interestingly, the plaque assays revealed an increase in the infectious viral titers in the presence of Ceramide C6, although viral RNA levels were similar to the DMSO control (Fig. 7E).

U87MG cells show improved Host-cell survival with Ag-126 treatment

We assessed whether Ag-126 treatment resulted in a reduction of cytopathic effects (CPE) in context of TC-83 infection. Our earlier experiments using host-based inhibitors of TC-83 multiplication have alluded to the possibility of increased survival of infected cells when the kinetics of viral multiplication are decreased

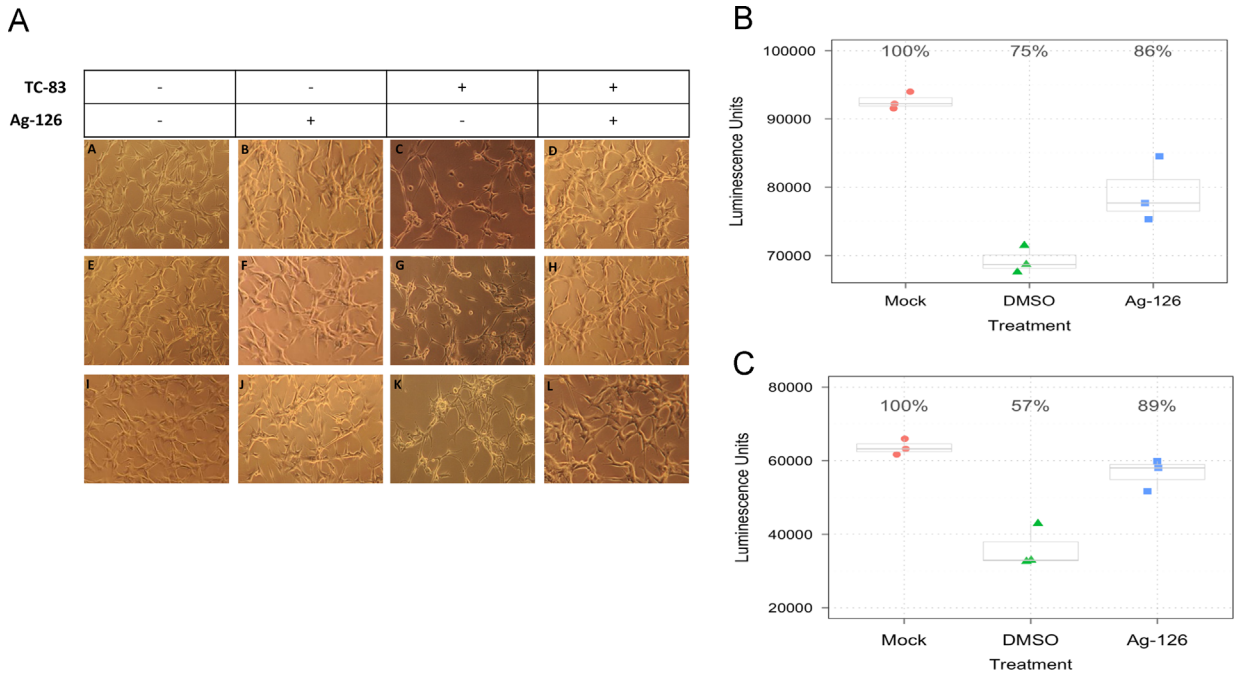

Fig. 8. Inhibition of ERK phosphorylation during TC-83 infection improves survival of U87MG cells. (A) U87MG cells were seeded in a 12-well plate and infected with TC-83 (MOI:1). Treatment of Ag-126 was included at 10 μM. DMSO was maintained as a negative control. Images were taken at 24 hpi, with controls being Ag-126 treatment alone and untreated uninfected cells. Rows A–D, E–H and I–L represent biological triplicate experiments. The conditions in each panel for every column are indicated in the table above the images. (B and C) U87MG cells were seeded in white walled 96 well plates and infected with TC-83, with or without Ag-126 treatments (10 μM). At 24 hpi (B) and 48 hpi (C), biological triplicate wells were subjected to Cell-Titer-Glo assay. *X*-axis indicates the amount of cell survival and *Y*-axis indicates the drug treatment conditions. All experiments were repeated three independent times.

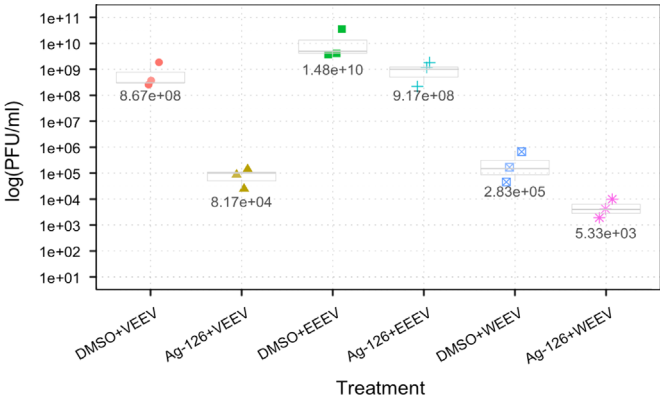

Fig. 9. Inhibition of ERK1/2 activation with Ag-126 reduces replication of virulent alphaviruses. U87MG cells were seeded in a 96 well format and pretreated for 2 h with Ag-126 (10 μM) or DMSO alone. The cells were infected with VEEV TrD, EEEV strain GA97, WEEV strain California 1930 (MOI:0.1). Supernatants collected at 24 hpi were quantified by plaque assay. *X*-axis refers to infectious viral titers and *Y*-axis indicates the nature of the virus and type of treatment that was used.

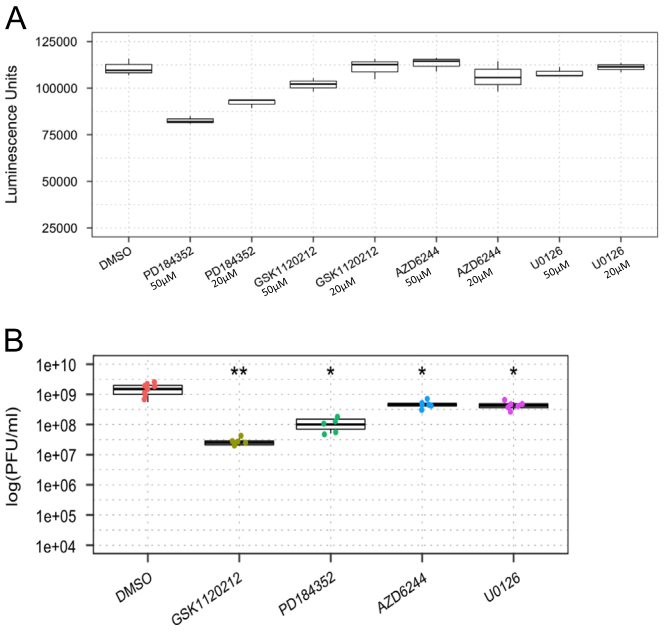

Fig. 10. Inhibition of MEK1/2 with small molecule inhibitors have different effects on TC-83 replication. (A) Toxicity was assessed at 24 h post-treatment by Cell-Titer-Glo assay. (B) U87MG cells were treated with the inhibitors for 2 h and then infected with TC-83 (MOI:0.1) for one hour. Supernatants collected at 24 hpi were subjected to plaque assay.

(Amaya et al., 2014). To test whether Ag-126 treatment reduced CPE in TC-83 infected U87MG cells, we imaged infected, untreated cells and infected, Ag-126-treated cells 24 hpi (Fig. 8A). The infected, Ag-126-treated cells (panels D, H and L) appeared to be healthier than the infected, untreated cells (panels C, G and K) and phenotypically resembled the mock infected, untreated cells (A, E and I). Ag-126 treatment by itself did not change the morphology of the cells (B, F and J) when compared to the mock infected, untreated cells. Next we adopted a quantitative cell survival assay to verify increased cell viability when treated with Ag-126. In the survival assay, we measured the fraction of live cells by Cell-Titer-Glo at 24 and 48 hpi in the presence and absence of Ag-126 (Fig. 8B and C). At 24 hpi, infected cells treated with DMSO alone dropped to 75% of the luminescence seen in the uninfected cells. However, Ag-126-treated cells showed 11% more luminescence when compared to DMSO alone. At 48 hpi, treated cells had 32% more survival than the DMSO alone control. Collectively, the data supports the idea that in conjunction with exerting antiviral

activity, inhibition of ERK phosphorylation during early stages of infection by inhibitors, such as Ag-126, can contribute to increasing survival of infected cells.

Ag-126 treatment down regulates viral multiplication of three virulent alphavirus strains

We extended our analysis of Ag-126 dependent inhibition of ERK1/2 phosphorylation to the virulent strains of New World alphaviruses. In this experiment, we utilized the Trinidad Donkey (TrD) strain of VEEV, the GA97 strain of EEEV, and the California 1930 strain of WEEV. To this end, U87MG cells were pretreated with DMSO or Ag-126 and then infected with each of the virulent strains. All infections were performed for 1-hour and conditioned media were replaced and the supernatants collected 24 h later. Plaque assays were performed to quantify infectious viral particles (Fig. 9). Addition of Ag-126 treatment reduced viral titers of VEEV TrD from 8.67×10^8 PFU/ml to 8.17×10^4 PFU/ml, a 4-log decrease. In the case of EEEV, treatment resulted in an overall 1-log drop, from 1.48×10^{10} PFU/ml to 9.17×10^8 PFU/ml. For WEEV, Ag-126 treatment contributed to a 2-log decrease in viral titer from 2.83×10^5 PFU/ml to 5.33×10^3 PFU/ml. The results supported the hypothesis that ERK1/2 was likely to be a broad-spectrum target for the development of antivirals against New World alphaviruses.

MEK1/2 inhibitors differ in their abilities to decrease TC-83 multiplication

Finally, we wanted to know if other inhibitors of the Ras–RAF–MEK–ERK signaling cascade would similarly affect VEEV multiplication. To this end, we employed various MEK1/2 inhibitors to characterize their effect on TC-83 multiplication in our cells. We chose to evaluate PD184352, GSK1120212, AZD6244, and U0126. Among these, GSK1120212 is already FDA approved for cancer therapy, and would therefore be a strong candidate to repurpose as an antiviral therapeutic for alphaviruses. The toxicity profile of each compound was evaluated at 50 and 20 μM concentrations in U87MG cells by Cell-Titer-Glo assay as described previously. PD184352 showed a significant decrease in cell viability to 74% at 50 μM treatment, but was relatively nontoxic at 20 μM (Fig. 10A). All other compounds were non-toxic at both concentrations. U87MG cells were then pre treated with 50 μM of each MEK inhibitor, except for PD184352 which was tested at 20 μM, and then infected with TC-83 virus. Supernatants were collected 24 h later and subjected to plaque assay. The results showed that GSK1120212 was able to decrease VEEV multiplication by up to 2 logs while AD184352 was also effective, but to a lesser extent. U0126 and AZD6244 were not effective at inhibiting TC-83 multiplication in this system (Fig. 10B). Cumulatively, our data indicated that inhibition of ERK1/2 signaling is an attractive option to inhibit alphavirus multiplication in human cells.

Discussion

Innate immune responses that are established early following exposure to infectious agents play an essential role in pathogen control and protection of the host. Such innate immune mechanisms are shaped by host phospho-signaling responses that undergo fairly elaborate modulation upon cellular insult, which includes exposure to infectious agents. Virus infection is well documented to activate many host signaling responses that often shift the balance between host survival and cell death. Many viruses have been known to hijack some of these intrinsic host responses to enable establishment of a productive viral infection. Often such hijacking mechanisms involve additional host responses that are also modified, cumulatively resulting in a suppressed host environment where the virus can multiply without interference by the innate host protective mechanisms such as interferon responses. In fact, New World alphaviruses including VEEV and WEEV have been known to suppress the host interferon response by a mechanism that involves the viral capsid protein (Atasheva et al., 2010; Peltier et al., 2013). As part of the pathogenesis, New World alphaviruses have also been known to trigger apoptosis of the infected cells, mediated by host signaling pathways (Griffin and Hardwick, 1997). Our previous studies using GSK-3β and IKK-β inhibitors have established that inhibition of host phospho-signaling events exerts an inhibitory effect on viral multiplication in infected human cells (Amaya et al., 2014; Kehn-Hall et al., 2012; Narayanan et al., 2012).

In the current study, we have provided evidence for the activation of ERK1/2 phosphorylation at early time points following exposure to the TC-83 strain of VEEV (Fig. 1). Our observation that phosphorylated ERK1/2 increased in TC-83 infected cells while there were no significant changes observed in the levels of total ERK1/2 protein indicated that the increase in phosphorylated forms was independent of de novo protein synthesis (Fig. 1C). Small molecule inhibitors of ERK1/2 phosphorylation, such as Ag-126, when used in the nontoxic range, have the potential to inhibit viral multiplication (Fig. 2). We have observed that the inhibition is mediated through interruption of potentially early and late events in the infectious process. Our data suggests that the compound is not directly virucidal. We hypothesize that Ag-126 is likely to interfere with a host process that is essential for the internalized virus to go through the subsequent steps of capsid shedding and release of viral nucleic acid into the cytoplasm of the cell. Additional steps in the inhibitory process may involve abberations in packaging and viral egress. Ongoing research to address these possibilities will include analysis of host events that are essential for the intracellular transport of the virus, which may involve cytoskeletal dynamics.

The hypothesis does not negate the possibility of direct ERK-mediated modification of viral proteins. For example, viral nonstructural proteins (nsPs) may be phosphorylated by host kinases that influence their function. One such alphavirus protein that is known to be heavily phosphorylated is nonstructural protein 3 (nsP3) (Li et al., 1990; Peränen et al., 1988; Vihinen and Saarinen, 2000). nsP3 is a critical regulator of negative strand synthesis and affects virulence. However, the exact role of nsP3 in the viral infectious cycle continues to remain unknown. Our earlier studies have indicated that nsP3 may be phosphorylated by IKK-β. We will be characterizing the phosphorylation status of nsP3 in the presence of inhibitors, such as Ag-126, because nsP3 contains other potential phosphorylation sites. These interesting aspects are currently under investigation in our laboratory. In addition, it appears that localization of E2 glycoprotein to the ER of infected cells may be affected by Ag-126 (Fig. 6). It is therefore interesting to speculate that Ag-126 may have an effect on viral particle assembly and packaging.

Our studies suggest that inhibition of ERK phosphorylation may also contribute to increase in survival of infected cells and decrease in CPE following alphavirus infection (Fig. 8). Viruses such as Varicella-Zoster virus (VZV) have been documented to control apoptosis of infected cells by modulating multiple aspects of the apoptotic signaling responses, often culminating in differential phosphorylation of key effector molecules like BAD, BAX, BIM, etc. (Liu and Cohen, 2014). Interestingly, it was demonstrated that the VZV protein ORF12 triggered the phosphorylation of ERK in order to inhibit apoptosis (Liu et al., 2012). It would be informative to quantify the status of various apoptotic events in VEEV-infected cells in the presence and absence of effective

inhibitors like Ag-126 to determine mechanisms that mediate cell death of infected cells.

Our observation that MEK and ERK are phosphorylated in VEEV-infected cells and ERK inhibitors effectively interfere with viral multiplication open the doors for FDA-approved MEK and ERK inhibitors including Trametinib, Selumetinib, and Cobemetinib, for repurposing as antivirals with a novel indication as New World alphavirus therapeutics. Repurposing such MEK and ERK inhibitors is additionally attractive because of our evidence that inhibition of ERK has a broad-spectrum effect on the multiplication of all three New World alphaviruses (Fig. 9). In our hands, at least one other FDA approved inhibitor of the MEK–ERK cascade was efficacious at inhibiting VEEV multiplication even though Ag-126 had a better inhibitory potential (Fig. 10).

The RPPA analysis identified many signaling nodes in the RAS-RAF-MEK-ERK signaling cascade as being phosphorylated in TC-83 infected cells. We have focused the current study only on ERK and its phosphorylation status. This study opens new avenues of exploration on the consequences of the phosphorylation of additional targets in this cascade on alphavirus replication. For example, p90RSK phosphorylation has been demonstrated to be intimately associated with replication of SARS-coronavirus (Mizutani et al., 2006). It would be interesting to determine whether inhibitors of these multiple ERK phospho-signaling nodes will exert a synergistic and more potent inhibition of the virus when used in a combinatorial capacity.

Methodology

Cell culture

Human astrocytoma cell (U87MG cells) and African green monkey kidney epithelial cells (VERO cells) were maintained in DMEM supplemented with 10% Fetal Bovine Serum (FBS), 1% Penicillin/Streptomycin, and 1% L-Glutamine at 37 °C and 5% CO_2.

Viral infections

Cells were seeded in a 96-well plate in order to attain confluence within 24 h. The media was removed prior to infection and saved and is referred to as conditioned media. The cells were infected for 1 h at 37 °C to allow for viral adsorption, and then the viral inoculum was removed. Cells were washed once with PBS, and the conditioned media replaced. Then the cells were incubated at 37 °C, 5% CO_2 overnight, and the supernatant collected 24 hpi and stored at −80 °C until analyzed.

Small molecule inhibitor/activator studies

Small molecules included Ag-126 (Santa Cruz Biotechnology, Catalogue No. sc-3528), Ceramide C6 (Santa Cruz Biotechnology, Catalogue no. sc-3527), U0126 (Cell Signaling Technology, Catalogue no. 9903), PD184352 (Selleckchem, Catalogue no. S1020), GSK1120212 (Selleckchem, Catalogue no. S2673), and AZD6244 (Selleckchem, Catalogue no. S1008). Compounds were dissolved in dimethyl sulfoxide (DMSO). U87MG cells were seeded in a 96-well plate at a density of 10,000 cells per well. The next day the cells were pretreated with the compound for 2 h. Drug concentrations were maintained in a manner that did not exceed 0.1% DMSO final concentration per well. The conditioned media containing the compound were removed and viral infections proceeded at multiplicity of infection (MOI) of 0.1 for 1 h at 37 °C. The viral inocula were then removed and replaced with the conditioned media with compound. The cells were incubated for 24 h at 37 °C, 5% CO_2, and the supernatant was collected and stored at −80 °C until analyzed.

Cell viability assays

Cell viability was measured using a Cell-Titer-Glo Luminescent Cell Viability kit (Promega, Catalog no. G7570) according to the manufacturer's instructions. Briefly, U87MG cells were seeded in 96-well white wall plates at 10,000 cells per well and incubated for 24 h at 37 °C, 5% CO_2. Cells were then treated with Ag-126 or DMSO (control) and incubated for 24 h at 37 °C, 5% CO_2. To determine cell viability, Cell-Titer-Glo reagent was added to the cells in a ratio of 1:1. The plate was shaken for 2 min at room temperature and then incubated for 10 min at room temperature. Luminescence was detected using the DTX 880 multimode detector (Beckman Coulter).

Reverse phase protein microarray (RPPA)

The methods for RPPA have been described previously (Popova et al., 2010a, 2010b). U87MG cells were plated in a 6-well format and infected with TC-83 (MOI:1) for one hour at 37 °C, 5% CO_2. After 6 h, the cells were washed with 1 × PBS, lysed and boiled for 10 min. The lysis buffer composition is as follows: 1:1 mixture of T-PER Reagent (Pierce, IL) and 2 × Tris–glycine SDS sample buffer (Novex, Invitrogen, CA) in the presence of 2.5% β -mercaptoethanol, and protease and phosphatase inhibitors (1 × Halt cocktail, Pierce). Lysed samples were stored at −80 °C until they were ready for the RPPA study. To conduct the RPPA study, approximately 30–50 nl of each sample were printed onto nitrocellulose slides (Whatman, MA) using a high-resolution 2470 arrayer (Aushon Biosystems, Billerica, MA). Randomly chosed slides were stained with CyproRuby stain to quantify total protein which will be used in signal normalization (described below). The printed slides were stained using a Dako Autostainer with specific antibodies using a biotin-linked peroxidase-catalyzed signal amplification (Dako, CSA kit). The slides were stained with a secondary biotinylated goat anti-rabbit IgG antibody (Vector Labs, Burlingame, CA) and imaged (Umax PowerLook III scanner, Umax, Dallas, TX). The images were analyzed with software AlphaAse FC (Alpha Innotech). For every antibody used, the average pixel intensity value for negative control (staining with second antibody only) was subtracted from the average pixel intensity value and normalized by the corresponding average value of the total protein intensity. The signal intensity for every antibody spot was statistically evaluated using GraphPad Prism ver5 software (Graphpad Software, CA). The antibodies used in RPPA array were against the following phosphorylated proteins and purchased from Cell Signaling: (catalog numbers of antibodies indicated in parenthesis): B-Raf c-Raf ERK (9101), MEK1/2 (9121), p65 (3031), p90RSK (9341), RSK3 (9348), STAT1 (9134),

Assays to observe cytopathic effects (CPE)

U87MG cells were seeded at a density of 1.0×10^5cells per well in a 12-well plate. Cells were mock-treated, treated with Ag-126, or treated with Ag-126 for 2 h and then infected for 1 h. Each condition was performed in triplicate wells. Random sections of each well were imaged at 24 hpi and 48 hpi using a Zeiss AXIOVERT-25 microscope with Pixera's Viewfinder 3.0 software.

Plaque assays

VERO cells were seeded at a density of 1.5×10^5cells per well in a 12-well plate. Viral supernatants, diluted in DMEM, were used to infect VERO cells in technical duplicate. The plates were incubated at 37 °C and 5% CO_2 for 1 h with occasional rocking. A 1 ml overlay comprised of 2XE-MEM and 0.6% agarose (1:1) was added to each of the wells. Once solidified the plates were incubated for an

additional 48 h at 37 °C and 5% CO_2. To complete the assay, an addition of a 10% Formaldehyde solution was added to the surface of the agarose plugs followed by 1 h incubation at room temperature. The plates were then rinsed with diH_2O and the agarose plugs removed. A 1% crystal violet solution containing 20% ethanol was added to each of the wells and incubated at room temperature with rocking for 30 min. The plates were rinsed with diH_2O, and visible plaques counted to determine viral titers as plaque forming units per ml (PFU/ml).

Modified plaque reduction neutralization assay

TC-83 viral stock at 1.6×10^7 PFU/ml was incubated at room temperature for 1 h either in the presence or absence of 10 μM Ag-126 with gentle mixing. Samples were then directly subjected to plaque assay.

Protein extract preparations for western blot analysis

In order to obtain whole cell lysates, the media was removed from U87MG cells and the cells were washed once with PBS. Next the cells were lysed with lysis buffer that consisted of a 1:1 mixture of T-PER reagent (Pierce, Catalogue no. 78510), 2 × Tris–glycine SDS sample buffer (Invitrogen, Catalogue no. LC2676), 2.5% β-mercaptoethanol, and protease and phosphatase inhibitor cocktail (1 × Halt mixture, Pierce). Cells with lysis buffer were incubated at room temperature for one minute, and then collected. Cell lysates were boiled for 10 min and stored at −80 °C until analyzed.

Quantitative RT-PCR (q-RT-PCR)

U87MG cells were pre-treated with 1 μM Ceramide C6 or 10 μM Ag126 for 2 h and then infected with TC-83 at an MOI: 0.1. As a control cells were treated with DMSO. At 16 h post infection cells were lysed using the MagMAX™-96 Total RNA Isolation Kit (Life Technologies, AM1830) as per the manufacturer's instructions. Intracellular viral RNA was quantitated using q-RT-PCR with primers and probe for nucleotides 7931–8005 of VEEV TC-83 (Kehn-Hall et al., 2012). The q-RT-PCR cycling conditions were as follows: 1 cycle at 50 °C for 30 min, 1 cycle at 95 °C for 2 min and 40 cycles at 95 °C for 15 s and 61 °C for 1 min using the StepOne Plus Real Time PCR system. The primer and probe pairs used were originally described by Julander; forward primer (TCTGACAAGACGTTCCCAATCA) and reverse primer (GAATAACTT CCCTCCGACCACA) and Taqman probe (5′ 6-carboxyfluorescein-TGTTGGAAGGGAAGATAAACGGCTACGC-6-carboxy- *N,N,N′,N′*-tetramethylrhodamine-3′) (Julander et al., 2008). The q-RT-PCR assays were performed using BioRad iTaq Universal Probes one-step 2 × mix (BioRad, 172–5140). The absolute quantification was calculated based on the threshold cycle (Ct) relative to the standard curve.

Western blot analysis

Whole cell lysates were separated on a 4–20% Tris–Glycine Gel at 100 V and transferred to a polyvinyl difluoride (PVDF) membrane using the iBlot gel transfer system (Invitrogen). The membranes were blocked in 1% dry milk in PBS-Tween 20 or 2% BSA in PBS-Tween 20 at room temperature. Primary antibodies to VEEV Capsid (BEI Resources, NR 9403), VEEV Glycoprotein (BEI Resources, NR 9404), p-ERK 1/2 (Thr 202/Tyr 204) (Cell Signaling Technology, Catalogue no. 4370), ERK 1/2 Antibody (Cell Signaling Technology, Catalogue no. 9102), p-p90RSK (Ser380) (Cell Signaling Technology, Catalogue no. 11,989) and HRP-conjugated actin (Abcam, Catalogue no. ab49900) were used according to manufacturer's instructions. The blots were incubated with primary antibody overnight at 4 °C. Following 2 washes with PBS-Tween 20 the blots were then incubated with respective secondary HRP-coupled antibody for 2 h. After 3 washes with PBS-Tween 20 and 1 wash with PBS, the membranes were visualized by chemiluminescence using SuperSignal West Femto Maximum Sensitivity Substrate Kit (ThermoScientific) on a BIO- RAD Molecular Imager ChemiDoc XRS system (BIO-RAD).

Immunofluorescence

U87MG cells were seeded at a density of 20,000 cells/well in an 8-well chambered slide. The cells were either, mock-treated, treated with 10 μM Ag-126 or infected with TC-83 at an MOI of 5. Cells were fixed with 4% paraformaldehyde for 20 min and permeabilized with 0.5% Triton X-100 in PBS for 15 min. Slides were washed with PBS and blocked at room temperature for 10 min with 3% BSA. The slides were incubated with primary antibody for 1 h in the dark at 37 °C, and then washed three times with PBS and incubated with respective secondary antibody Alexa Fluor antibodies (Invitrogen) for 1 h in the dark at 37 °C. Primary antibody markers for the endoplasmic reticulum and golgi included PDI (C81H6) and RCAS1 (D2B6N), respectively (Cell Signaling Technology, Catalogue no. 8653S). Slides were washed three times with PBS and incubated with DAPI for 10 min in the dark at room temperature. Following an additional PBS wash, the slides were mounted with Fluoromount G (SouthernBiotech, Catalogue no. 0100-01) and stored in the dark at 4 °C overnight. The cells were imaged using Nikon Eclipse TE2000-U. Images were taken at 60 × objective.

Statistical analysis

Graphing and data analyses were performed using the R Statistical Language. We performed three independent experiments using separately harvested viral supernatants each time. Each experiment included three biological samples per group. We recorded the raw plaque counts for each of the plaque assays and determined the PFU/ml. The figures present scatter plots overlaid on box and whisker plots. The box and whisker plots have their conventional meanings. We use our graphical representations as well as performing Wilcoxon rank sum tests to assess differences among treatment groups. *P*-values less than 0.01 were considered statistically significant. Significant results are indicated on the figures in the following fashion: $P\text{-value} \leq 0.0001$ (***), $P\text{-value} \leq 0.001$ (**), $P\text{-value} \leq 0.01$ (*).

Acknowledgments

VEEV pTC83 was a kind gift from Ilya Frolov of the University of Alabama at Birmingham. The following reagents were obtained through the NIH Biodefense and Emerging Infections Research Resources Repository, NIAID, NIH: (i) Venezuelan Equine Encephalitis Virus, TC83 (Subtype IAB), NR63, (ii) Venezuelan equine encephalitis virus Trinidad Donkey (subtype IA/B), NR-332, (iii) Polyclonal Anti-Venezuelan Equine Encephalitis Virus, TC83 (Subtype IA/B) Capsid Protein (antiserum, Goat), NR-9403, (iv) Polyclonal Anti-Venezuelan Equine Encephalitis Virus, TC-83 (Subtype IA/B) Glycoprotein (antiserum, Goat), NR-9404. We are thankful for the following reagent, which was obtained from Dr. Jonathan Jacobs from MRIGlobal: EEEV GA97. The following reagent was obtained from ATCC: WEEV (California 1930 strain), VR-70. We would like to thank Jyoti Shankar from the J Craig Venter Institute for providing statistical programming mentorship to KV.

References

Amaya, M., Voss, K., Sampey, G., Senina, S., de la Fuente, C., Mueller, C., Calvert, V., Kehn-Hall, K., Carpenter, C., Kashanchi, F., Bailey, C., Mogelsvang, S., Petricoin, E., Narayanan, A., 2014. The role of IKKβ in venezuelan equine encephalitis virus infection. PLoS One 9, e86745. http://dx.doi.org/10.1371/journal.pone.0086745.

Atasheva, S., Krendelchtchikova, V., Liopo, A., Frolova, E., Frolov, I., 2010. Interplay of acute and persistent infections caused by Venezuelan equine encephalitis virus encoding mutated capsid protein. J. Virol. 84, 10004–10015. http://dx.doi.org/10.1128/JVI.01151-10.

Barrett, Alan D.T., Stanberry, Lawrence R. (Eds.), 2009. Preface. In: Vaccines for Biodefense and Emerging and Neglected Diseases. Academic Press, London, p. xvii, ISBN: 9780123694089, 〈http://dx.doi.org/10.1016/B978-0-12-369408-9.00079-2〉.

Boldogh, I., AbuBakar, S., Albrecht, T., 1990. Activation of proto-oncogenes: an immediate early event in human cytomegalovirus infection. Science 247, 561–564.

Burke, C.W., Gardner, C.L., Steffan, J.J., Ryman, K.D., Klimstra, W.B., 2009. Characteristics of alpha/beta interferon induction after infection of murine fibroblasts with wild-type and mutant alphaviruses. Virology 395, 121–132. http://dx.doi.org/10.1016/j.virol.2009.08.039.

Cai, Y., Liu, Y., Zhang, X., 2007. Suppression of coronavirus replication by inhibition of the MEK signaling pathway. J. Virol. 81, 446–456. http://dx.doi.org/10.1128/JVI.01705-06.

Canonico, P.G., Kende, M., Luscri, B.J., Huggins, J.W., 1984. In-vivo activity of antivirals against exotic RNA viral infections. J. Antimicrob. Chemother. 14, 27–41. http://dx.doi.org/10.1093/jac/14.suppl_A.27.

Carrera, J.-P., Forrester, N., Wang, E., Vittor, A.Y., Haddow, A.D., López-Vergès, S., Abadía, I., Castaño, E., Sosa, N., Báez, C., Estripeaut, D., Díaz, Y., Beltrán, D., Cisneros, J., Cedeño, H.G., Travassos da Rosa, A.P., Hernandez, H., Martínez-Torres, A.O., Tesh, R.B., Weaver, S.C., 2013. Eastern equine encephalitis in Latin America. N. Engl. J. Med. 369, 732–744. http://dx.doi.org/10.1056/NEJMoa1212628.

Carter, A.B., Hunninghake, G.W., 2000. A constitutive active MEK – > ERK pathway negatively regulates NF-kappa B-dependent gene expression by modulating TATA-binding protein phosphorylation. J. Biol. Chem. 275, 27858–27864. http://dx.doi.org/10.1074/jbc.M003599200.

Chatterjee, P.K., Patel, N.S.A., Kvale, E.O., Brown, P.A.J., Stewart, K.N., Britti, D., Cuzzocrea, S., Mota-Filipe, H., Thiemermann, C., 2003. The tyrosine kinase inhibitor tyrphostin AG126 reduces renal ischemia/reperfusion injury in the rat. Kidney Int. 64, 1605–1619. http://dx.doi.org/10.1046/j.1523-1755.2003.00254.x.

Chuderland, D., Seger, R., 2005. Protein–protein interactions in the regulation of the extracellular signal-regulated kinase. Mol. Biotechnol. 29, 57–74. http://dx.doi.org/10.1385/MB:29:1:57.

Cruzalegui, F.H., Cano, E., Treisman, R., 1999. ERK activation induces phosphorylation of Elk-1 at multiple S/T-P motifs to high stoichiometry. Oncogene 18, 7948–7957. http://dx.doi.org/10.1038/sj.onc.1203362.

Fine, D.L., Jenkins, E., Martin, S.S., Glass, P., Parker, M.D., Grimm, B., 2010. A multisystem approach for development and evaluation of inactivated vaccines for Venezuelan equine encephalitis virus (VEEV). J. Virol. Methods 163, 424–432. http://dx.doi.org/10.1016/j.jviromet.2009.11.006.

Furler, R.L., Uittenbogaart, C.H., 2010. Signaling through the P38 and ERK pathways: a common link between HIV replication and the immune response. Immunol. Res. 48, 99–109. http://dx.doi.org/10.1007/s12026-010-8170-1.

Garmashova, N., Gorchakov, R., Volkova, E., Paessler, S., Frolova, E., Frolov, I., 2007. The old world and new world alphaviruses use different virus-specific proteins for induction of transcriptional shutoff. J. Virol. 81, 2472–2484. http://dx.doi.org/10.1128/JVI.02073-06.

Griffin, D.E., Hardwick, J.M., 1997. Regulators of apoptosis on the road to persistent alphavirus infection. Annu. Rev. Microbiol. 51, 565–592. http://dx.doi.org/10.1146/annurev.micro.51.1.565.

Hans, A., Syan, S., Crosio, C., Sassone-Corsi, P., Brahic, M., Gonzalez-Dunia, D., 2001. Borna disease virus persistent infection activates mitogen-activated protein kinase and blocks neuronal differentiation of PC12 Cells. J. Biol. Chem. 276, 7258–7265.

Hong, S.-K., Yoon, S., Moelling, C., Arthan, D., Park, J.-I., 2009. Noncatalytic function of ERK1/2 can promote Raf/MEK/ERK-mediated growth arrest signaling. J. Biol. Chem. 284, 33006–33018. http://dx.doi.org/10.1074/jbc.M109.012591.

Hu, P., Han, Z., Couvillon, A.D., Exton, J.H., 2004. Critical role of endogenous Akt/IAPs and MEK1/ERK pathways in counteracting endoplasmic reticulum stress-induced cell death. J. Biol. Chem. 279, 49420–49429. http://dx.doi.org/10.1074/jbc.M407700200.

Jacqué, J.M., Mann, A., Enslen, H., Sharova, N., Brichacek, B., Davis, R.J., Stevenson, M., 1998. Modulation of HIV-1 infectivity by MAPK, a virion-associated kinase. EMBO J. 17, 2607–2618. http://dx.doi.org/10.1093/emboj/17.9.2607.

Johnson, R.A., Ma, X.L., Yurochko, A.D., Huang, E.S., 2001. The role of MKK1/2 kinase activity in human cytomegalovirus infection. J. Gen. Virol. 82, 493–497.

Julander, J.G., Skirpstunas, R., Siddharthan, V., Shafer, K., Hoopes, J.D., Smee, D.F., Morrey, J.D., 2008. C3H/HeN mouse model for the evaluation of antiviral agents for the treatment of Venezuelan equine encephalitis virus infection. Antiviral Res. 78, 230–241. http://dx.doi.org/10.1016/j.antiviral.2008.01.007.

Kehn-Hall, K., Narayanan, A., Lundberg, L., Sampey, G., Pinkham, C., Guendel, I., Van Duyne, R., Senina, S., Schultz, K.L., Stavale, E., Aman, M.J., Bailey, C., Kashanchi, F., 2012. Modulation of GSK-3β activity in Venezuelan equine encephalitis virus infection. PLoS One 7, e34761. http://dx.doi.org/10.1371/journal.pone.0034761.

Li, G.P., La Starza, M.W., Hardy, W.R., Strauss, J.H., Rice, C.M., 1990. Phosphorylation of Sindbis virus nsP3 in vivo and in vitro. Virology 179, 416–427.

Liu, X., Cohen, J.I., 2014. Inhibition of Bim enhances replication of varicella-zoster virus and delays plaque formation in virus-infected cells. J. Virol. 88, 1381–1388. http://dx.doi.org/10.1128/JVI.01695-13.

Liu, X., Li, Q., Dowdell, K., Fischer, E.R., Cohen, J.I., 2012. Varicella-Zoster virus ORF12 protein triggers phosphorylation of ERK1/2 and inhibits apoptosis. J. Virol. 86, 3143–3151. http://dx.doi.org/10.1128/JVI.06923-11.

Luo, H., Yanagawa, B., Zhang, J., Luo, Z., Zhang, M., Esfandiarei, M., Carthy, C., Wilson, J.E., Yang, D., McManus, B.M., 2002. Coxsackievirus B3 replication is reduced by inhibition of the extracellular signal-regulated kinase (ERK) signaling pathway. J. Virol. 76, 3365–3373.

Martin, S.S., Bakken, R.R., Lind, C.M., Garcia, P., Jenkins, E., Glass, P.J., Parker, M.D., Hart, M.K., Fine, D.L., 2010. Evaluation of formalin inactivated V3526 virus with adjuvant as a next generation vaccine candidate for Venezuelan equine encephalitis virus. Vaccine 28, 3143–3151. http://dx.doi.org/10.1016/j.vaccine.2010.02.056.

Mizutani, T., Fukushi, S., Saijo, M., Kurane, I., Morikawa, S., 2006. Regulation of p90RSK phosphorylation by SARS-CoV infection in Vero E6 cells. FEBS Lett. 580, 1417–1424. http://dx.doi.org/10.1016/j.febslet.2006.01.066.

Narayanan, A., Kehn-Hall, K., Senina, S., Lundberg, L., Van Duyne, R., Guendel, I., Das, R., Baer, A., Bethel, L., Turell, M., Hartman, A.L., Das, B., Bailey, C., Kashanchi, F., 2012. Curcumin inhibits Rift valley fever virus replication in human cells. J. Biol. Chem. 287, 33198–33214. http://dx.doi.org/10.1074/jbc.M112.356535.

Novogrodsky, A., Vanichkin, A., Patya, M., Gazit, A., Osherov, N., Levitzki, A., 1994. Prevention of lipopolysaccharide-induced lethal toxicity by tyrosine kinase inhibitors. Science 264, 1319–1322.

Paessler, S., Weaver, S.C., 2009. Vaccines for Venezuelan equine encephalitis. Vaccine 27 (Suppl. 4), SD80–SD85. http://dx.doi.org/10.1016/j.vaccine.2009.07.095.

Parra, J.L., Buxadé, M., Proud, C.G., 2005. Features of the catalytic domains and C termini of the MAPK signal-integrating kinases Mnk1 and Mnk2 determine their differing activities and regulatory properties. J. Biol. Chem. 280, 37623–37633. http://dx.doi.org/10.1074/jbc.M508356200.

Peltier, D.C., Lazear, H.M., Farmer, J.R., Diamond, M.S., Miller, D.J., 2013. Neurotropic arboviruses induce interferon regulatory factor 3-mediated neuronal responses that are cytoprotective, interferon independent, and inhibited by Western equine encephalitis virus capsid. J. Virol. 87, 1821–1833. http://dx.doi.org/10.1128/JVI.02858-12.

Peränen, J., Takkinen, K., Kalkkinen, N., Kääriäinen, L., 1988. Semliki forest virus-specific non-structural protein nsP3 is a phosphoprotein. J. Gen. Virol. 69 (9), 2165–2178 (Pt).

Planz, O., Pleschka, S., Ludwig, S., 2001. MEK-specific inhibitor U0126 blocks spread of Borna disease virus in cultured cells. J. Virol. 75, 4871–4877. http://dx.doi.org/10.1128/JVI.75.10.4871-4877.2001.

Pleschka, S., 2008. RNA viruses and the mitogenic Raf/MEK/ERK signal transduction cascade. Biol. Chem. 389, 1273–1282. http://dx.doi.org/10.1515/BC.2008.145.

Pleschka, S., Wolff, T., Ehrhardt, C., Hobom, G., Planz, O., Rapp, U.R., Ludwig, S., 2001. Influenza virus propagation is impaired by inhibition of the Raf/MEK/ERK signalling cascade. Nat. Cell Biol. 3, 301–305. http://dx.doi.org/10.1038/35060098.

Popova, T.G., Turell, M.J., Espina, V., Kehn-Hall, K., Kidd, J., Narayanan, A., Liotta, L., Petricoin 3rd, E.F., Kashanchi, F., Bailey, C., Popov, S.G., 2010a. Reverse-phase phosphoproteome analysis of signaling pathways induced by Rift valley fever virus in human small airway epithelial cells. PLoS One 5, e13805. http://dx.doi.org/10.1371/journal.pone.0013805.

Popova, T.G., Turell, M.J., Espina, V., Kehn-Hall, K., Kidd, J., Narayanan, A., Liotta, L., Petricoin, E.F., Kashanchi, F., Bailey, C., Popov, S.G., 2010b. Reverse-phase phosphoproteome analysis of signaling pathways induced by Rift valley fever virus in human small airway epithelial cells. PLoS One, 5. http://dx.doi.org/10.1371/journal.pone.0013805.

Raines, M.A., Kolesnick, R.N., Golde, D.W., 1993. Sphingomyelinase and ceramide activate mitogen-activated protein kinase in myeloid HL-60 cells. J. Biol. Chem. 268, 14572–14575.

Rodríguez, M.E., Brunetti, J.E., Wachsman, M.B., Scolaro, L.A., Castilla, V., 2014. Raf/MEK/ERK pathway activation is required for Junin virus replication. J. Gen. Virol. , http://dx.doi.org/10.1099/vir.0.061242-0.

Roskoski Jr, R., 2012a. ERK1/2 MAP kinases: structure, function, and regulation. Pharmacol. Res. Off. J. Ital. Pharmacol. Soc 66, 105–143. http://dx.doi.org/10.1016/j.phrs.2012.04.005.

Roskoski Jr, R., 2012b. MEK1/2 dual-specificity protein kinases: structure and regulation. Biochem. Biophys. Res. Commun. 417, 5–10. http://dx.doi.org/10.1016/j.bbrc.2011.11.145.

Sharma, A., Bhattacharya, B., Puri, R.K., Maheshwari, R.K., 2008. Venezuelan equine encephalitis virus infection causes modulation of inflammatory and immune response genes in mouse brain. BMC Genomics 9, 289. http://dx.doi.org/10.1186/1471-2164-9-289.

Sharma, A., Gupta, P., Glass, P.J., Parker, M.D., Maheshwari, R.K., 2011. Safety and protective efficacy of INA-inactivated Venezuelan equine encephalitis virus: implication in vaccine development. Vaccine 29, 953–959. http://dx.doi.org/10.1016/j.vaccine.2010.11.033.

Shaul, Y.D., Seger, R., 2007. The MEK/ERK cascade: from signaling specificity to diverse functions. Biochim. Biophys. Acta 1773, 1213–1226. http://dx.doi.org/10.1016/j.bbamcr.2006.10.005.

Snyder, A.J., Mukhopadhyay, S., 2012. The alphavirus E3 glycoprotein functions in a clade-specific manner. J. Virol. 86, 13609–13620. http://dx.doi.org/10.1128/JVI.01805-12.

Vihinen, H., Saarinen, J., 2000. Phosphorylation site analysis of semliki forest virus nonstructural protein 3. J. Biol. Chem. 275, 27775–27783. http://dx.doi.org/10.1074/jbc.M002195200.

Volkova, E., Frolova, E., Darwin, J., Forrester, N.L., Weaver, S.C., Frolov, I., 2008. IRES-dependent replication of Venezuelan equine encephalitis virus makes it highly attenuated and incapable of replicating in mosquito cells. Virology 377, 160–169. http://dx.doi.org/10.1016/j.virol.2008.04.020.

Weaver, S.C., Reisen, W.K., 2010. Present and future arboviral threats. Antiviral Res. 85, 328. http://dx.doi.org/10.1016/j.antiviral.2009.10.008.

Wulfkuhle, J.D., Edmiston, K.H., Liotta, L.A., Petricoin 3rd, E.F., 2006. Technology insight: pharmacoproteomics for cancer–promises of patient-tailored medicine using protein microarrays. Nat. Clin. Pract. Oncol. 3, 256–268. http://dx.doi.org/10.1038/ncponc0485.

Xing, Z., Cardona, C.J., Anunciacion, J., Adams, S., Dao, N., 2010. Roles of the ERK MAPK in the regulation of proinflammatory and apoptotic responses in chicken macrophages infected with H9N2 avian influenza virus. J. Gen. Virol. 91, 343–351. http://dx.doi.org/10.1099/vir.0.015578-0.

Yoon, S., Seger, R., 2006. The extracellular signal-regulated kinase: multiple substrates regulate diverse cellular functions. Growth Factors Church Switz. 24, 21–44. http://dx.doi.org/10.1080/02699050500284218.

Zacks, M.A., Paessler, S., 2010. Encephalitic alphaviruses. Vet. Microbiol. 140, 281. http://dx.doi.org/10.1016/j.vetmic.2009.08.023.

Zhang, Y., Cho, Y.-Y., Petersen, B.L., Zhu, F., Dong, Z., 2004. Evidence of STAT1 phosphorylation modulated by MAPKs, MEK1 and MSK1. Carcinogenesis 25, 1165–1175. http://dx.doi.org/10.1093/carcin/bgh115.